Check for updates

e+i elektrotechnik und informationstechnik

Online monitoring method based on magnetic field for stator insulation lifetime tests

Lukas Weisenseel [ID] · Dennis Sieling · Daniel Dietz [ID] · Jochen Rittmaier · Martin Doppelbauer

Abstract In this paper, an online monitoring method of insulation faults based on the stator magnetic field for insulation life tests is developed. In recent years, a trend towards higher operating voltages, higher switching frequencies, and shorter voltage rise times has been observed for low-voltage motors, mainly driven by increasing electromobility. An insulation system must withstand these requirements over the entire operating range and the required service life. Significant over-dimensioning of the insulation is not justifiable, since this has a negative impact on the utilization or the efficiency of the machine. Lifetime tests are therefore required for dimensioning the insulation. For this purpose, end-of-life (EOL) tests are usually carried out. Here, different damage patterns occur, which are distinguished during the analysis. In addition to the EOL test, insulation faults can be detected by monitoring the magnetic field of a stator during the operating time ("online"). An early shutdown often prevents the drive from further damage. In this paper, five methods to evaluate the magnetic field are presented. The operation is investigated using a 2D FEM simulation (sinus excitation) and a network simulation (PWM excitation) and evaluated through measurements on a 4 kW PM external rotor stator. Subsequently, an application of the method on a test rig setup with continuous monitoring of the insulation system is presented. The test setup serves as a basis for future investigations on the influence of voltage rise time, switching frequency, and DC link voltage on insulation faults to estimate the lifetime of insulation systems of electrical machines.

Online-Überwachungsmethode auf Basis des magnetischen Felds für Statorisolations-Lebensdauertests

Zusammenfassung In diesem Beitrag wird eine Online-Überwachungsmethode von Isolationsfehlern auf Basis des Statormagnetfelds für Isolationslebensdauertests entwickelt. In den vergangenen Jahren ist bei Niederspannungsmotoren ein Trend in Richtung höherer Betriebsspannungen, höherer Schaltfrequenzen und kurzen Spannungsanstiegszeiten, vor allem getrieben durch die zunehmende Elektromobilität, festzustellen. Diesen Anforderungen muss ein Isolationssystem über den kompletten Betriebsbereich und die geforderte Lebensdauer standhalten. Eine starke Überdimensionierung der Isolation ist dabei nicht vertretbar, da diese sich negativ auf die Ausnutzung bzw. den Wirkungsgrad der Maschine auswirkt. Zur Dimensionierung der Isolation werden daher Lebensdauertests benötigt. In der Regel werden hierfür End-of-Life(EOL)-Tests durchgeführt. Hierbei treten verschiedene Schadbilder auf, die bei der Analyse differenziert werden. Ergänzend zum EOL-Test können Isolationsfehler durch die Überwachung des Magnetfelds eines Stators während der Betriebszeit ("online") erkannt werden. Das frühzeitige Abschalten ermöglicht eine Fehlersuche im frühen Stadium des Ausfalls. In diesem Beitrag werden fünf Möglichkeiten zur Auswertung des magnetischen Felds vorgestellt. Die

L. Weisenseel (✉) · D. Sieling · D. Dietz · J. Rittmaier
ebm-papst Mulfingen GmbH & Co. KG,
Bachmühle 2, 74673 Mulfingen, Germany
lukas.weisenseel@de.ebmpapst.com

L. Weisenseel · M. Doppelbauer
Karlsruher Institut für Technologie,
Engelbert-Arnold-Straße 5, 76161 Karlsruhe, Germany

Funktionsweise wird anhand einer 2D-FEM-Simulation (Sinus-Anregung) und einer Netzwerksimulation (PWM-Anregung) untersucht und durch Messungen an einem 4-kW-PM-Außenläuferstator abgeglichen. Im Anschluss wird eine Anwendung des Verfahrens auf einem Prüfstandsaufbau bei kontinuierlicher Überwachung des Isolationssystems vorgestellt. Der Versuchsaufbau dient als Basis für künftige Untersuchungen zum Einfluss von Spannungsanstiegszeit, Schaltfrequenz und Zwischenkreisspannung auf Isolationsfehler zur Abschätzung der Lebensdauer von Isolationssystemen elektrischer Maschinen.

Schlüsselwörter Online-Monitoring · Isolationsfestigkeit · Windungsschluss · Isolationssystem · Isolations-Lebensdauer

Nomenclature

AD	Agnalog-to-digital
ADC	Analog-to-digital converter
DC	Direct current
DUT	Device under test
EOL	End-of-life
FEM	Finite element method
GUI	Graphical user interface
ITF	Inter-turn fault
LAN	Local Area Network
PA	Polyamide
PCB	Printed circuit board
PET	Polyethylene terephthalate
PWM	Pulse-width modulation

1 Introduction

The insulation system of electric machines is subject to a variety of stresses that have a decisive influence on its lifetime, especially at inverter operation [7]. In addition to electrical stresses, mechanical and thermal loads, but also certain environmental influences can lead to a reduction in the insulation quality [2]. In extreme cases, this can lead to shutdown of machines and equipment, resulting in costly production downtime. An insulation fault in the motor winding leads to severe overheating at the defect [6, 8] which may show up as a discoloration of the insulating material or as a melted winding. The insulation fault spreads further across the winding and leads to destruction of the electric motor. In order to investigate the cause of failure of a stator, it is necessary to switch it off as early as possible in case of failure. Based on the defect [1], the analysis can be carried out. The use of inverter-fed machines continues to increase due to rising requirements for system efficiency [5]. With increasing efficiency higher power densities are targeted for more compact drive solutions [9]. In novel power electronics, fast-switching semiconductors based on silicon carbide (SiC) are used, enabling increased switching frequencies and shorter voltage risetimes (above $70\,\mathrm{kV\,\mu s^{-1}}$). To reduce the power dissipation of electric converters, electric motors are operated at increased voltage slope dU/dt. In addition, to increase charging power in electric cars, DC link voltages increases. However, these optimizations impose novel loads on the insulation system of electric motors [7]. For the design of electrical machines, knowledge of the electrical stress and the resulting damage is of great interest. To be able to investigate the stress on the insulation system of electric motors in detail, lifetime tests have to be done. For this purpose, test rigs are required, enabling continuous condition monitoring of the stator winding insulation system. In the insulation lifetime tests carried out, the rotor is left out. This is due to the fact that the test effort can be significantly reduced, as no load machines are required to brake the tested stators. The stators are set to the test temperature by ohmic losses in the motor winding. As a result, the heat is generated directly at the insulation system. The inductance of the tested motor (external rotor motors with concentrated winding, see Sect. 2.1), changes only slightly by leaving out the rotor. Therefore the voltage transients will also behave similar to real operation. In real operation the induced voltage of the rotor in a windung with interturn fault (ITF) accelerates aging and leads to rapid failure. The target of the test is to determine the failure mode, therefore the acceleration of a failure is rather of secondary importance. The complete structure of the test is shown in Fig. 15.

The paper is structured as follows. Sect. 2 introduces the test specimen under consideration and the available detection methods. The is examined in more detail in Sect. 3 by creating an equivalent circuit diagram and an FEM simulation. In addition, the transient operation of the method is examined with of a equivalent circuit simulation and the results are compared with measurements. In Sect. 4, a test bench is presented in which the detection method was implemented and which is used for the development of the insulation system of inverter-fed electric machines. In Sect. 5 the content of the paper is resumed.

2 Online insulation fault detection method

In this Section, the mechanism of the monitoring method of insulation faults is presented. In the first part, the stator is described, to which the procedure is applied. In the second part, the mechanism of the detection method is pointed out.

2.1 Investigated Stator

The device under test (DUT) is a stator of an 4 kW external rotor motor with a tooth coil winding (Fig. 1). The diameter of the stator is 112 mm and the insulation system of this stator consists of the three following parts:

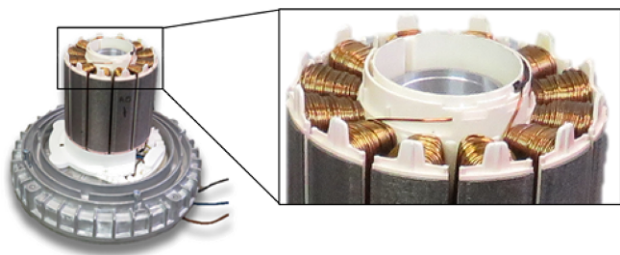The **ground insulation** is a plastic coating of the lamination stack increasing the insulation quality be-

Fig. 1 DUT – stator of an external rotor motor

tween winding and stator iron. The **phase insulation** is often made of air, although it is replaced by insulating paper (PET, PA polymer) or plastic inlays in higher voltage applications. It shields the motor from critical electrical field strengths between closely spaced wires of different phases within the slot. The **turn insulation** (enameled copper wire coating) usually consists of a combination of polyesterimide and poliamidimide.

2.2 Principle insulation detection method via the magnetic field

The method presented in [3, 5, 6] enables detecting an insulation via the magnetic field. Five options (1), (2), (3), (4), (5) of detecting insulation faults via (stray) magnetic fields are identified and presented in Fig. 2 and described in Sect. 2.2.1. In [5, 6] only the methods (1) and (4) were examined.

2.2.1 Sensor winding
Compared to a "healthy" winding, the voltage induced in the sensor winding is reduced upon the occurrence of an insulation fault. The voltage induced in the sensor winding shows a reduction upon the occurrence of an insulation fault. This principle works with one sensor winding, but the sensitivity increases with the number of turns.

2.2.2 Contacting the lamination stack
By contacting the iron sheet package of one stator tooth as seen in Fig. 2, it is possible to measure a voltage induced by the eddy currents. The presence of

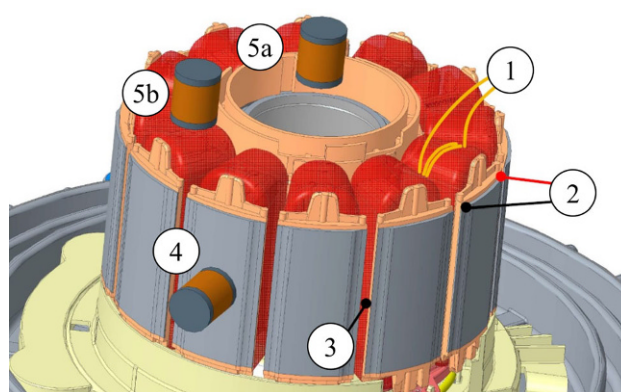Fig. 3 Storage coil with ferrite core used as sensor coil [10]

Fig. 2 Options for detecting an insulation fault via the magnetic stator field (1 – sensor winding, 2 – contacting the lamination stack, 3 – air gap planar coil, 4 – sensor coil mounted to the stator tooth 5 – sensor coil/magnetic field sensor placed above excitation coil or in stator center point)

an insulation fault is measurable by a reduced voltage value.

2.2.3 Air gap planar coil
A planar coil (e.g. a printed circuit coil), is placed in a stator slot. The induced voltage in this coil shows a significant change in the occurrence of an insulation fault.

2.2.4 Sensor coil mounted to the stator tooth
A coil, e.g. storage inductance (Fig. 3) placed radial on the outer site of the stator tooth (Fig. 2 – no. 4) Due to its simplicity this method is suited as end-of-line test for stator insulation systems, but not for complete motors.

2.2.5 Sensor coil placed (a) axially in the stator end winding region or (b) in the center point on top of the stator (bearing socket)
This method is very similar to the one in Sect. 2.2.4. However, the magnetic field is not evaluated directly at the stator tooth. (a) For the first option the sensor coil is axially displaced in the stator end winding region. This way, the stray field above one excitation coil can be measured and evaluated. (b) For the second option the sensor coil is placed on top of the stator in the center (bearing socket). Thus, the magnetic stray field of all stator tooth windings affects the induced voltage in the sensor coil. It is a convenient detection method for the entire stator insulation. However, the localisation of the insulation fault is not possible compared to (a).

3 Theoretical Background

To understand the functionality of the detection method 4 from Sect. 2.2.4 is used as an example to examine it in more detail below.

In Fig. 4, the structure is shown as a horizontal cut through the stator. There are three different coils that
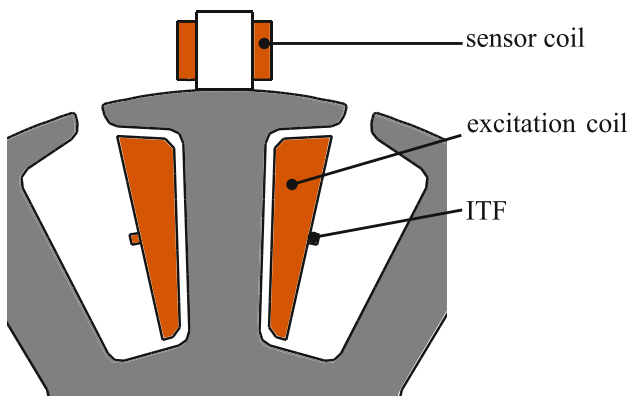
Fig. 4 2D schematic representation of the stator insulation fault detector with sensor coil mounted to the stator tooth (Fig. 2 – no. 4) – sensor coil ($L_{Sens}, R_{Sens}, N_{Sens}$), excitation coil ($L_W, R_W, N_W$), ITF ($N_{ITF}$)

Fig. 5 Magnetic circuit of the given structure

have an influence on the system. The excitation coil (= part of the stator winding, subscript: W) provides the magnetic field. The sensor coil (subscript: Sens) is similar to the storage coil in Fig. 3. The insulation fault is represented by a one-turn short-circuited rectangular coil (subscript: ITF). In this paper the ITF is used to demontrate the function of the presented methods. Also phase insulation and ground insulation faults lead to changes in the magnetic flux and thus also in the magnetic field. The functionalitiy of the methods for these faults were investigated but not shown in this paper.

An electric motor consists of a stator and a rotor. The magnetic flux passes from the laminated stack via the air gap into the rotor and closes via the backiron. If the stator is energized without a rotor, the magnetic flux according to Figs. 6 and 7 closes via the stator slots to the adjacent teeth. Also, the flux passes through the sensor coil and the surrounding air into the two adjacent stator teeth. The simplified magnetic circuit is shown in Fig. 5.

Fig. 5 includes the flux linkages $\Psi_W, \Psi_{Sens}, \Psi_{ITF}$ of the three coils from Fig. 4. Note that the excitation coil is excited by an impressed voltage as boundary condition, leading to the flux linkage Ψ_W. The flux linkage Ψ_{Sens}, respectively the induced voltage, is determined to distinguish between "healthy" and "unhealthy" coils. The flux linkage Ψ_{ITF} in the short-circuited winding leads to a flux in the opposite direction to Ψ_W. This flux results from a current excited by an induced voltage in the winding (1) (Faraday's law [4]).

$$\oint_{\delta A} \vec{E} d\vec{s} = -\int_A \frac{\partial \vec{B}}{\partial t} \cdot d\vec{A} \tag{1}$$

3.1 FEM simulation of the magnetic field

To investigate the exact courses of the field lines in the given arrangement, a magnetically linear 2-dimensional finite element method (2D FEM) simulation
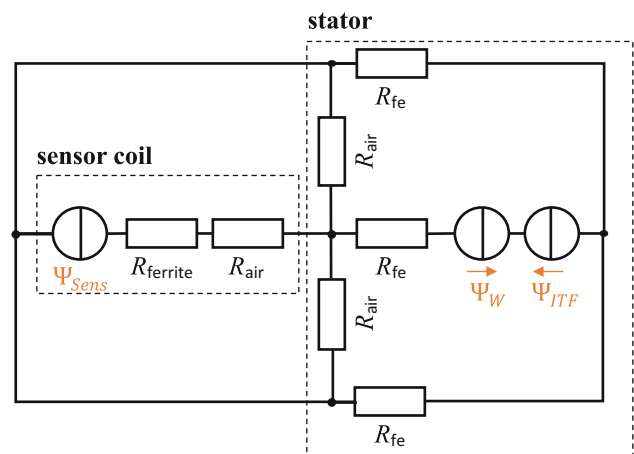
was carried out, neglecting the iron saturation. The boundary conditions of the simulated arrangements are shown in Table 1.

The magnetic field lines of this arrangement can be seen in Fig. 6. The model was simulated harmonically with an excitation of a $f = 20\,kHz$ sinusoidal voltage. In this application the main field passes through the neighboring teeth, but some field lines also pass through the sensor coil.

To show the effects of an ITF in Fig. 7 the field line plot of the structure with short-circuited winding is plotted. When an ITF is simulated, the part labeled with ITF in Fig. 4 is defined as short-circuited. Therefore, a current is driven by the induced voltage. As visible in Fig. 7, a magnetic field is created at the position of the ITF which counteracts the field of the excitation coil.

This counter field leads to a deflection of the main field of the excitation coil by the ITF. Two effects result from this distortion: The first effect is the reduction of the inductance L_W of the excitation coil, given by (2) [4], since the flux linkage is reduced by the counteracting flux of the ITF.

$$L_W = \frac{\Psi_W}{I_W} \tag{2}$$

The consequence of this is a decrease of the inductive reactance $X_W = \omega \cdot L_W$. This in turn leads to

Table 1 Input values 2D FEM simulation

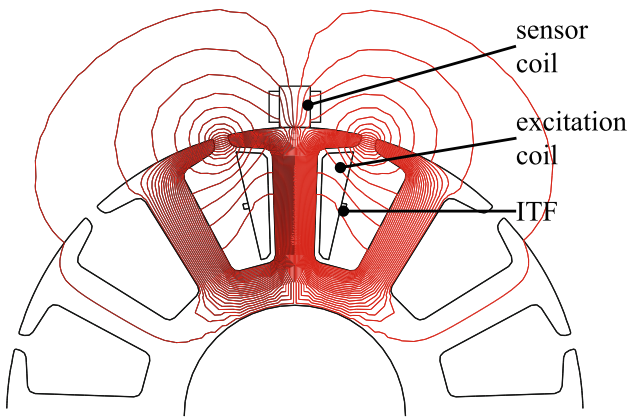|	
N_W / N_{Sens} / N_{ITF}	200 / 100 / 1
L_W / L_{Sens}	37 mH /2 mH both measured at 10 kHz (LCR 1707 Smart Tweezer)
R_W / R_{Sens}	4 Ω /2 Ω measured at 20 °C
$\mu_{r,fe}$ / $\mu_{r,ferrite}$	1000 / 10 000 $\frac{Vs}{Am}$
U_W	50 V $\cdot \cos(2\pi f t)$
Sensor coil dimensions	6 mm, 6 mm, 8 mm
Stator diameter	112 mm

Fig. 6 Simulated magnetic field line plot at 20 kHz sinusoidal voltage U_W without ITF
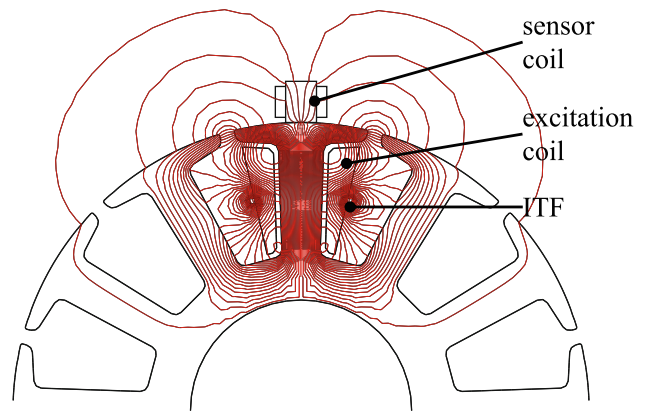

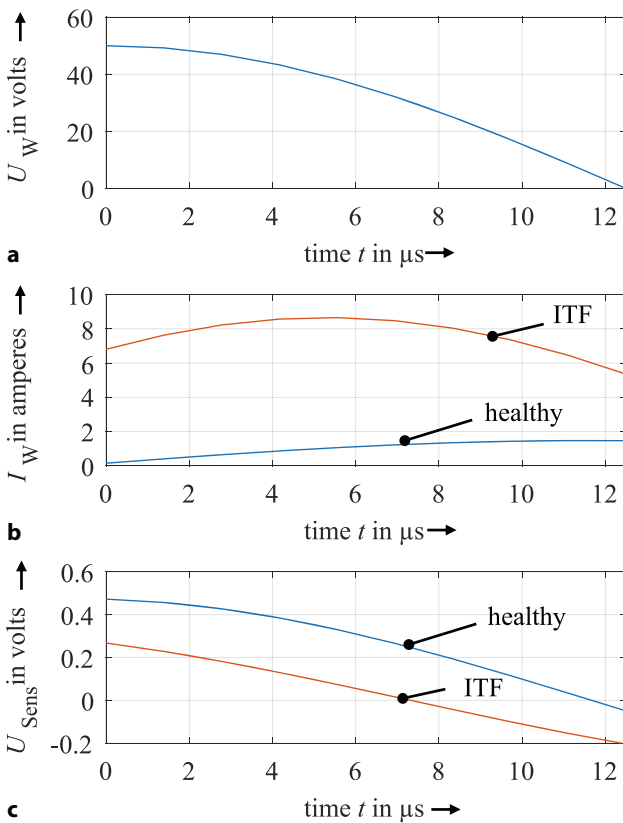Fig. 7 Simulated magnetic field line plot at 20 kHz sinusoidal voltage U_W with ITF

Fig. 8 Input and output variables of the FEM simulation at $U_W = 50$ V and $f = 20$ kHz – **a** excitation voltage U_W, **b** excitation currents I_W, **c** sensor voltages U_{Sens}

often fails quickly after the occurrence of a winding short circuit. The increased current due to an ITF also causes the magnetic flux of the excitation coil to increase. The deviation in phase shift of the current I_W with ITF is also due to the decrease in inductance. The decrease in inductance leads to a reduction of the phase shift from I_W to the voltage U_W. The second effect is visible in the shape of the voltage U_{Sens} in Fig. 8c. The voltages U_{Sens} with and without ITF show a significant difference in their maxima. At $t = 0$ by the occurrence of an ITF, U_{Sens} decreases by 50 % in comparison to a "healthy" winding. Obviously, this shows that a reduction of the flux Ψ_W also leads to a reduction of the induced voltage U_{Sens} in the winding. In conclusion, we have two effects which counteract each other. Comparing the two effects with Fig. 5, one understands that a balance is established between the magnetic flux increasing in the excitation coil due to the ITF and the opposing flux of the turn closure itself. Depending on the arrangement, there is an increase or decrease in the induced voltage U_{Sens} caused by an ITF. This depends on e.g. the geometry of the arrangement, the electrical parameters (voltage, frequency, shape), the temperature. In the tests carried out, a reduction in the induced voltage U_{Sens} triggered by an ITF occurred in most cases.

an increase of $I_W = U_W / X_W$ in the excitation coil. This effect is also visible in the result of the FEM simulation. Fig. 8 shows the values of U_W, I_W and U_{Sens} over time. Comparing the excitation currents I_W in Fig. 8b with and without ITF, a deviation in the amplitude as well as in the phase shift is detected. The peak value of I_W with ITF is four times higher than the current of the "healthy" winding. From this, a considerable impact of an ITF on the current and the local loss distribution is recognized why an electrical machine

Table 2 Input values equivalent circuit simulation

Simulation time	120 µs
Time step	10 ns
Solver	Backward euler
N_W / N_{Sens} / N_{ITF}	200 / 100 / 1
k_1 / k_2 / k_3	0.9 / 0.2 / 0.2
L_W / L_{Sens}	37 mH / 2 mH both measured at 10 kHz (*LCR 1707 Smart Tweezer*)
R_W / R_{Sens}	4 Ω / 2 Ω measured at 20 °C
$U_{W,Sinus}$ / $U_{W,PWM,Max}$	5V·cos(2πft) / 10 V at 10% duty cycle

Springer
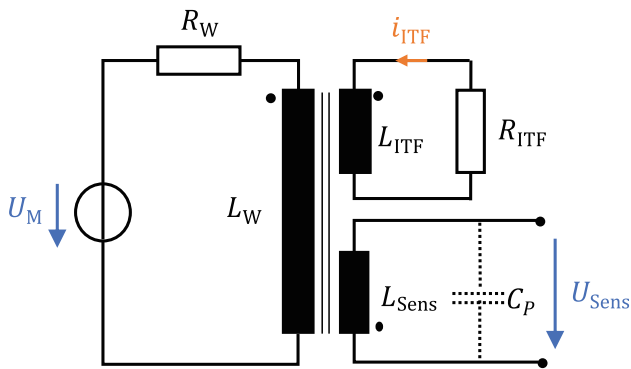
Fig. 9 Equivalent circuit model of the ITF (simulation model)

Fig. 10 Measurement setup, consisting of a digital oscilloscope (*R & S RTB* bandwidth: 1 GHz), a function generator (*Keysight 3321DA*) and the sensor coil (37 mH) and the DUT

3.2 Equivalent circuit simulation to investigate the behavior with PWM voltage

In the FEM simulation in Sect. 3.1 pure sinusoidal voltage feeding was considered. To evaluate the influence of a pulse width modulated (PWM) voltage U_W, which represents the inverter feeding of the considered stator, a transient time domain simulation in *GeckoCircuits* was conducted, using the equivalent circuit from Fig. 9. The boundary conditions of the simulation are given in Table 2. The model consists of the excitation coil (inductance L_W), the sensor coil (inductance L_{Sens}) and the short-circuited coil (inductance L_{ITF}), which are coupled magnetically. The equivalent circuit is given in Fig. 9. It is based on the principle of a transformer with two secondary windings. One of the secondary windings is short-circuited and represents the ITF.

For the simulation the winding resistance R_W, the winding inductance L_W of the excitation coil and the winding inductance L_{Sens} of the sensor coil were determined by measurement (*LCR 1707 Smart Tweezer*). The magnetic coupling is implemented via three coupling factors. This is exemplarily defined by the following formula for the coupling factor k_1 between excitation coil to ITF coil with M_1, being the mutual inductance of the two coils.

$$M_1 = k_1 \cdot \sqrt{L_W \cdot L_{ITF}} \tag{3}$$

The coupling factors k_1 – excitation coil to ITF, k_2 – excitation coil to sensor coil, k_3 – ITF to sensor coil, are determined by the FEM simulation (Sect. 3.1). The resistance of the ITF was estimated by $R_{ITF} = R_W/N_W = 20\,\mathrm{m\Omega}$ and the inductance by $L_{ITF} = L_W/N_W^2 = 0.925\,\mathrm{\mu H}$. The model was built twice, once with the short-circuited winding (ITF) and once with an open winding.

3.3 Comparison of Simulation/Measurement

To evaluate the simulation model from Sect. 3.2, a single stator coil of the DUT (Fig. 1) is supplied
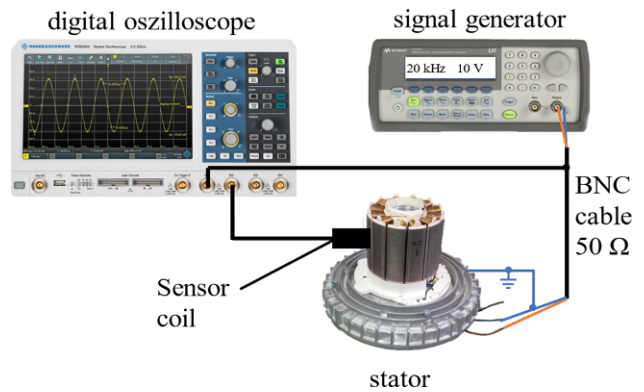
with a pure sinusoidal voltage generated by a signal generator (Fig. 10).

The sensor coil is placed at the stator tooth and the induced voltage is measured with an oscilloscope. The measurement devices and the stator are set to the same ground potential. The ITF is created manually by shorting two windings. The parameters are the same as in Sect. 3.1, except of the sinusoidal voltage U_W which is set to 5 V (Table 2) at 20 kHz by a signal generator. Fig. 11 shows the results.
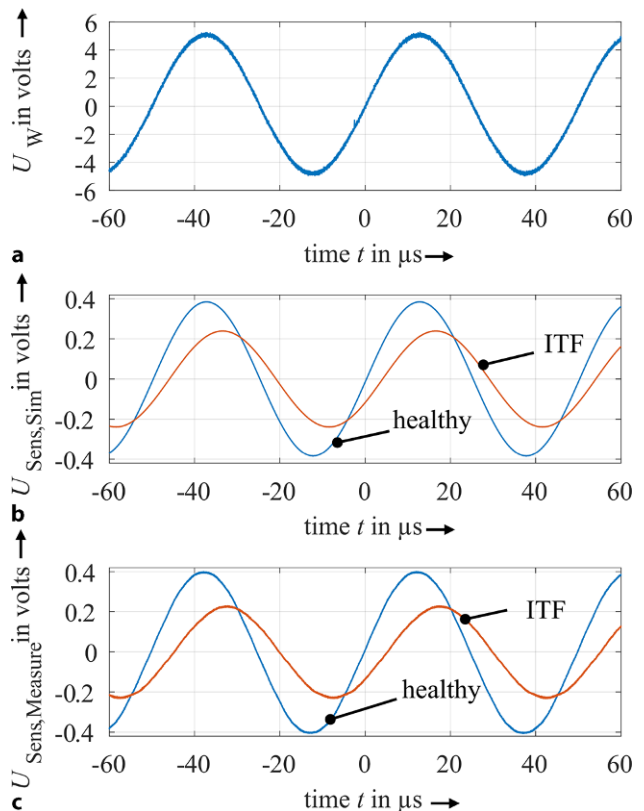

Fig. 11 Comparison of the simulation and the measurement of the effects of an ITF on the sensor voltage with sinusoidal supply voltage at 20 kHz – **a** sinusoidal supply voltage, **b** simulation result, **c** measurement result
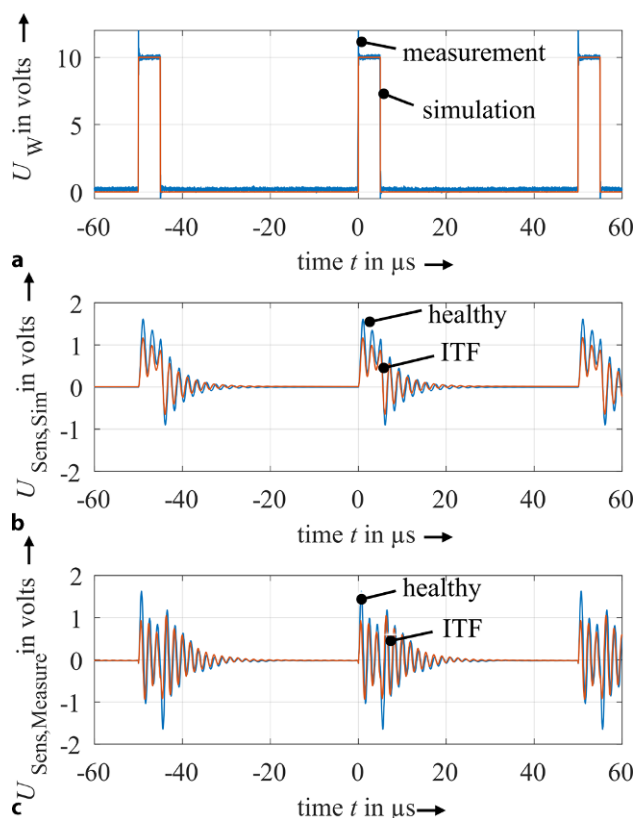
Fig. 12 Comparison of the measurement and simulation of the effects of an ITF on the sensor voltage with PWM supply voltage at 20 kHz – **a** excitaition signal, **b** simulated sensor voltage, **c** measured sensor voltage

In Fig. 11a the excitation voltage U_W is shown. The two resulting curves of the voltage U_{Sens} are shown in part (b) for the simulation and in part (c) for the measurement. Fig. 11b and c shows a good agreement between measurement and simulation for both cases with and without ITF, verifying the FEM model from Figs. 6 and 7. The small deviation can be neglected, since parasitic influences, such as the influence of parasitic capacitances, were not considered in the simulation. Thus, it can be concluded that the measured voltage at the sensor coil is sensitive to parameters such as the position and number of short-circuited turns, the temperature, the magnetic saturation state of the stator iron and the localization of the sensor coil. The next step is to verify how the model behaves with voltage pulses/PWM feeding. For this purpose, the identical setup as for the adjustment of the sinusoidal voltage was used (Fig. 10). The duty cycle of the rectangular pulse pattern with 10 V amplitude is exemplarily chosen to be 10 % (Fig. 12a. To simulate the settling process of the signal, a parasitic capacity C_P (Fig. 9) of 20 pF is set in parallel to L_{Sens}. C_P is dimensioned so that the same ringing frequency as the measurement occurs. The simulation result is shown in Fig. 12 in comparison to the measurements with the setup from Fig. 10. In (a) the excitation voltage U_W is plotted, whereas in b and c the sensor voltage

U_{Sens} of simulation and measurement are plotted. The result shows a reduction of the sensor voltage due to an ITF, as already shown in the FEM simulation in Sect. 3.1. Measurement and simulation tend to show a similar curve, however there are differences in the oscillation amplitude of the signals. Also, the time constant of the decaying process is slightly different. These effects can be attributed to the influence of parasitic capacitances and inductances. Even in the plot of U_W in part (a), the effect triggered by parasitic capacitances and inductances at the voltage overshoot of the measurement is visible. The switching action both with rising and falling edge is clearly visible in the curves b and c.

The results from this chapter show that the measurement results with the chosen setup have been confirmed by simulation. The main influencing variables could be determined: k_1, ratio of k_2 and k_3, L_W, R_W, C_P. It is therefore, possible to evaluate these influencing factors based on simulations in advance to a measurement setup.

4 Design of the measurement setup for endurance stress test

It has been shown in previous investigations that the method of magnetic field measurement is a very sensitive method to detect insulation faults reliable at a very early stage. In experiments [5] it was found that an ITF with only one short-circuited winding is clearly detected in the stray flux. Therefore, the method is very well suited to continuously monitor endurance tests and to be able to disconnect and examine the DUTs at a very early stage of insulation fault. Therefore, a method was developed to evaluate this effect and to apply it in an automated test routine. The automated insulation fault detector is used for insulation lifetime tests without stator.

4.1 Measuring process of the insulation fault detector

For a lifetime test, an easy-to-handle detection method is of advantage. After no. 4 from Fig. 2 is used for theoretical study and demonstration of the operation, no. 5b from Fig. 2 is used in this chapter in the application of a lifetime test. The operation and the resulting signal are similar to those described in the previous chapters. However, with this setup all coils can be monitored at the same time because the stray field of all excitation coils overlap in the center of the stator. The disadvantage is that it is no longer possible to determine which winding has a defect. This must be analyzed afterwards, e.g. with the setup no. 4 from Fig. 2. The evaluation principle works similar to that in [5]. The function process contains three steps (Fig. 13).

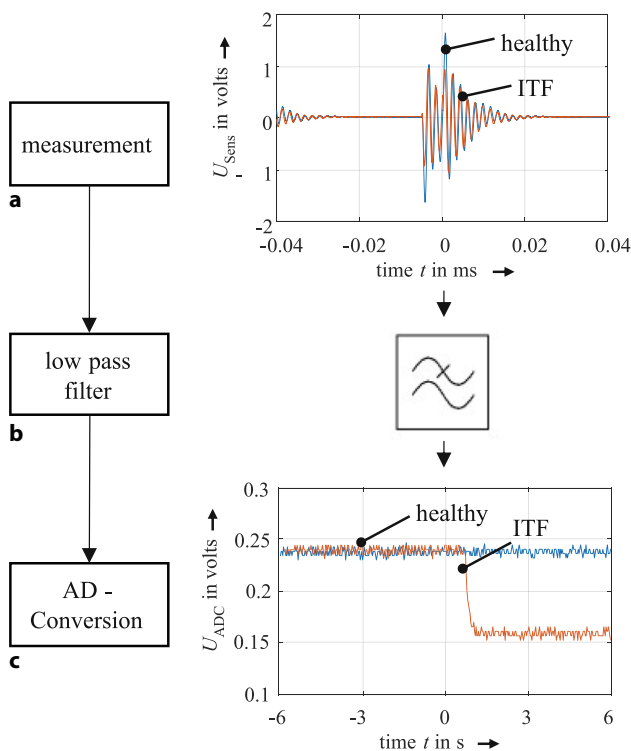The measurement is carried out via the measuring probe (storage coil from Fig. 3). This coil is centered in

Fig. 13 Measuring process of the insulation fault Detector (measurement – sensor coil, low pass filter – filter PCB, AD-Conversion – 12-Bit Arduino Due) – **a** mesurement signal of the sensor coil, **b** low pass filter generates mean value, **c** AD-converted signal with and without simulated ITF (drop in the waveform) to show functionality
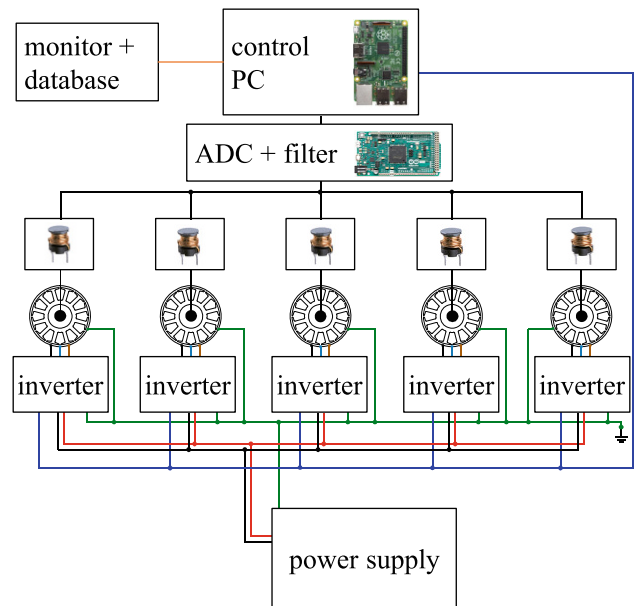

Fig. 14 Structure of the complete testbench for 5 stators with option no. 5 from Sect. 2.2.5
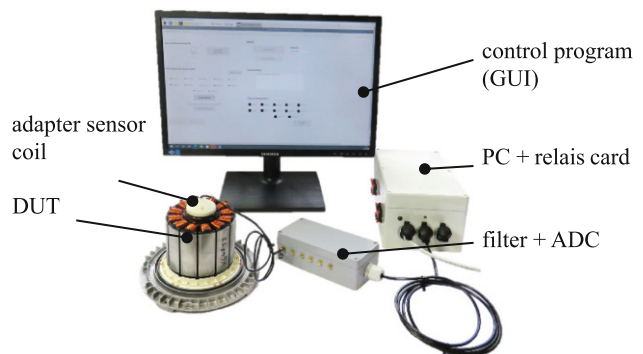

Fig. 15 Monitoring system for lifetime tests consisting of control program (GUI), PC and shutdown unit, filter and ADC unit, sensor coil with adaptation, DUT

the bearing seat of the stator with 3D-printed adapter (Fig. 15). The central position is required to couple the sensor coil symmetrically with the magnetic flux of the excitation coils. This way, the voltage at the sensor coil is induced in the same way by all excitation coils, for a possible insulation fault. The induced signal in the sensor coil is shown in Fig. 13a. Tis pulses result from the excitation voltage PWM. The measurement signal is filtered by a two-stage low-pass filter in the second step. The filter is set to the cutoff frequencies $f_{g1} = 1.6\,\text{Hz}$ and $f_{g2} = 350\,\text{Hz}$. The frequencies are set low because a signal as free of noise as possible is required for the evaluation (mean value). On the one hand, this allows the signal to be sampled by a microcontroller at a much lower sampling frequency than an oscilloscope. On the other hand, it enables defining a voltage threshold value $U_{\text{ADC,lim}}$ from which one defines the DUT as failed. The third step is the analogue-digital (AD)-conversion of the filtered signal. For that a 12 Bit ADC of an *Arduino Due* is used. The ADC output signal is shown at the bottom of Fig. 13. This signal curve forms the filtered signal of thousands of measured pulses (Fig. 13a). An insulation fault leads to a decrease (drops in the waveform with ITF, Fig. 13c) in the signal of sensor coil U_{Sens}. If this signal is smoothened, this decrease can be seen directly in the shape of the voltage U_{ADC}.

4.2 Automation of the measurement method

To evaluate whether the stator insulation is "healthy" or "unhealthy", it is necessary to define a threshold value. This value is stored in an initialization before the start of the insulation test. All subsequently recorded values (measured, filtered, AD-converted as in Fig. 13) are compared with this value. The decision of whether a stator passes the test is based on the percentage deviation that is defined for this measurement. When the threshold is exceeded, the stator in the test bench is automatically de-energized via an enable pin of the inverter. The measured values as well as the running time of the stator are written to a database. An overview of the complete test bench is shown in Fig. 14.

For the control of the testbench a *Raspberry Pi 3B* is used. Also, the test mode can be set up via a GUI (Fig. 15). Here the parameters shutdown threshold,

data of the measured stators and the threshold value are accessible. The GUI also shows the current status of the test. The measurement values combined with the stator data is sent by LAN to a central PC where the data is stored in a database. This way, many stator insulations can be tested at the same time, e.g. included in an end-of-line test.

5 Conclusions

In this report, a method for online monitoring of insulation faults by monitoring the magnetic field was studied in detail. For this purpose, possible measurement options based on this method were shown. It turned out that measurement principles based on the evaluation of the magnetic field can be used for the fault monitoring of lifetime tests. The theoretical background and the mode of operation was investigated by using method (4) from Fig. 2. The mode of operation of method (4) was derived with the help of an 2D FEM model. In addition to this, an equivalent circuit model was built up to simulate the operation for different excitation signals, such as PWM voltages. The equivalent circuit simulation results matched the measurement results well. An application of the online insulation fault monitoring routine is presented. It is proposed to generate the measuring signal by a measuring coil, to filter this signal afterwards and to compare the resulting signal with a defined threshold value. As a result, a failed stator can be switched off at an early stage during a life time test. This can be done for a large number of stators at the same time. Afterwards, the test specimen can be removed and examined without being completely destroyed. With the right selection of test specimens, the failure mechanisms of a stator can be determined.

References

1. DIN EN 60034-18-41:2014-11: Qualifizierung und Qualitätsprüfungen für teilentladungsfreie elektrische Isoliersysteme (Typ I) in drehenden elektrischen Maschinen, die von Spannungsumrichtern gespeist werden. IEC 60034-18-41:2014, Deutsche Fassung EN 60034-18-41:2014

2. DIN EN 60505 VDE 0302-1:2005-08 (IEC 60505:2004): Bewertung und Kennzeichnung von elektrischen Isoliersystemen

3. Gurusamy V, Bostanci E, Li C, Qi Y, Akin B (2021) A stray magnetic flux-based robust diagnosis method for detection and location of interturn short circuit fault in PMSM. IEEE Trans Instrum Meas 70:1–11

4. Ida N (2021) Engineering electromagnetics. Springer, Cham

5. Lee ST, Kim KT, Hur J (2015) Diagnosis technique for stator winding inter-turn fault in BLDC motor using detection coil. In: International Conference on Power Electronics and ECCE Asia (ICPE-ECCE Asia), pp 2925–2931

6. Mohammed A, Melecio JI, Djurovic S (2019) Stator winding fault thermal signature monitoring and analysis by *in situ* FBG sensors. IEEE Trans Ind Electron 66(10):8082–8092

7. Pauli F, Yang L, Schröder M, Hameyer K (2019) Lebensdauerabschätzung von Wicklungsisolierstoffsystemen in SiC-betriebenen elektrischen Niederspannungsmaschinen. Elektrotech Inftech 136(2):175–183

8. Pyrhonen J, Jokinen T, Hrabovcová V (2014) Design of rotating electrical machines, second edition edn. Wiley, Chichester

9. Weisenseel L, Sieling D, Güdelhöfer J (2020) Increasing the reproducibility of impulse PD measurements and development of an online interturn fault monitoring routine for external rotor motors. In: 2020 International Conference on Electrical Machines (ICEM), vol 1, pp 1356–1362

10. WE-TI Tonneninduktivität | Passive Bauelemente | Würth Elektronik Produktkatalog. https://www.we-online.com/de/components/products/WE-TI. Accessed Feb. 07, 2022
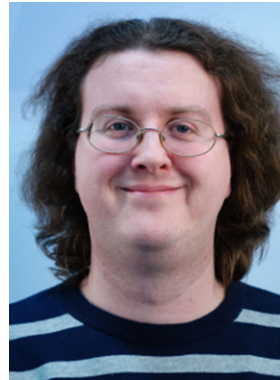
Lukas Weisenseel, received the M. Sc. degree in electrical engineering from University of Applied Science Heilbronn Campus Künzelsau, Germany in 2018. Since 2014 he has been working in the advanced development electronics and motor platform development with ebm-papst Mulfingen GmbH & Co. KG.

Dennis Sieling, received the B. Sc. Degree in physics at Bircham International University Madrid. Since 2019, he has been working in the motor platform development with ebm-papst Mulfingen GmbH & Co. KG.

Jochen Rittmaier, received the M. Sc. Degree in electrical engineering at Heilbronn University of Applied Sciences, Campus Künzelsau. Since 2011, he has been working in the motor advanced development at ebm-papst Mulfingen GmbH & Co. KG.

Daniel Dietz, studied industrial engineering at the Technical University of Darmstadt. Between 2016 and 2021, he worked as research associate at the Institute for Electrical Energy Conversion at the Technical University of Darmstadt and graduated with Dr.-Ing. degree in 2022. Since 2021 he is with ebm-papst Mulfingen GmbH & Co. KG.

Martin Doppelbauer, received the Dipl.-Ing. and Dr.-Ing. degrees in electrical engineering from the University of Dortmund, Dortmund, Germany, in 1990 and 1995, respectively. He was a Senior Manager for electric motor development with Danfoss Bauer, Esslingen, Germany, and SEW Eurodrive, Bruchsal, Germany. He has been a professor of hybrid electric vehicles with the Karlsruhe Institute of Technology, Karlsruhe, Germany, since 2011.